DFT Study of the Reaction between VO_2^+ and C_2H_6

L. Gracia, J. Andrés,* V. S. Safont, and A. Beltrán

Departament de Ciències Experimentals, Universitat Jaume I, Box 224, 12080 Castelló, Spain

J. R. Sambrano

Laboratório de Simulação Molecular, DM, Universidade Estadual Paulista, Box 473, 17033-360 Bauru, SP, Brazil

Received October 1, 2003

The molecular mechanisms of the reaction VO_2^+ ($^1A_1/^3A''$) + C_2H_6 (^1A_g) to yield $V(OH)_2^+$ ($^1\Sigma^+/^3\Sigma^-$) + C_2H_4 (^1A_g) and/or VO^+ ($^1\Delta$ / $^3\Sigma$) + H_2O ($^1A_1$) + C_2H_4 (^1A_g) have been investigated with density functional theory (DFT) at the B3LYP/6-311G(2d,p) level. Calculations including geometry optimization, vibrational analysis, and Gibbs free energy for the stationary points on the reactive potential energy surfaces at both the singlet (s) and first excited triplet (t) electronic states have been carried out. The most thermodynamically and kinetically favorable pathway is the formation of t-$V(OH)_2^+$ + C_2H_4 along a four-step molecular mechanism (insertion, two consecutive hydrogen transfers, and elimination). A crossing point between s and t electronic states has been characterized. A comparison with previous works on VO_2^+ + C_2H_4 (Gracia et al. *J. Phys. Chem. A* **2003**, *107*, 3107−3120) and VO_2^+ + C_3H_8 (Engeser et al. *Organometallics* **2003**, *22*, 3933−3943) reactions allows us a rationalization of the different reactivity patterns. The catalytic role of water molecules in the tautomerization process between hydrated oxide cation, $VO(H_2O)^+$, and dihydroxide cation, $V(OH)_2^+$, is achieved by a water-assisted mechanism.

1. Introduction

Chemical reactivity involving transition metal oxides has gained increasing interest in the last years due to the promising role that these chemical processes can play and their widespread use in heterogeneous catalysis, exhibiting high selectivity and activity.[1,2] Gas-phase studies provide mechanistic insight into the elementary steps of reactions at a molecular level,[3,4] and the reactions between transition metal oxides and hydrocarbons have been of particular interest to gas-phase chemical kineticists and dynamicists because of their importance in catalytic processes.[5−7] These reactions often involve C−H and/or C−C bond activation followed by elimination of hydrogen or small alkane groups.[8−10] Therefore, the knowledge about microscopic physical and chemical properties of materials based on metal oxides is of great importance. In particular, the molecular mechanisms related with chemical rearrangements involving transition metal compounds are not easy to determine by experimental procedures, and DFT methods offer a possible alternative to overcome this difficulty. These systems can be regarded as suitable models to investigate the elementary steps involved in industrial catalysis because clusters of different sizes and compositions often form the surface structure of heterogeneous catalysts.

The application of quantum mechanical calculations to these compounds is more difficult than to other branches of chemistry[11−14] because many reactions of transition metal oxides involve low lying excited electronic states. In these cases, the corresponding stationary points governing chemical reactivity lie on different potential energy surfaces (PESs), and this fact opens the possibility of a nonadiabatic behavior, in which the most favorable pathway does not remain on a single PES.

Reactions that involve a change in the spin state and thus occur on two or more PESs are known to be important in determining the outcome of chemical processes.[15−17] In particular, this type of chemical

* Corresponding author. Tel: +34 964 728072. Fax: +34 964728066. E-mail: andres@exp.uji.es.

(1) Henrich, V. E.; Cox, P. A. *The Surface Science of Metal Oxides*; Cambridge University Press: New York, 1994; Vol. 45.
(2) Rao, C. N. R. *Transition Metal Oxides*; VCH: New York, 1995.
(3) Schröder, D.; Shaik, S.; Schwarz, H. *Acc. Chem. Res.* **2000**, *33*, 139−145.
(4) Ogliaro, F.; Harris, N.; Cohen, S.; Filatov, M.; de Visser, S. P.; Shaik, S. *J. Am. Chem. Soc.* **2000**, *122*, 8977−8989.
(5) Oyama, S. T.; Hightower, J. W. *Catalytic Selective Oxidation*; American Chemical Society: Washington, DC, 1993.
(6) Warren, D. K.; Oyama, S. *Heterogeneous Hydrocarbon Oxidation*; American Chemical Society: Washington, DC, 1996.
(7) Argyle, M. D.; Chen, K. D.; Bell, A. T.; Iglesia, E. *J. Phys. Chem. B* **2002**, *106*, 5421−5427.
(8) Vankoppen, P. A. M.; Brodbeltlustig, J.; Bowers, M. T.; Dearden, D. V.; Beauchamp, J. L.; Fisher, E. R.; Armentrout, P. B. *J. Am. Chem. Soc.* **1990**, *112*, 5663−5665.
(9) Vankoppen, P. A. M.; Brodbeltlustig, J.; Bowers, M. T.; Dearden, D. V.; Beauchamp, J. L.; Fisher, E. R.; Armentrout, P. B. *J. Am. Chem. Soc.* **1991**, *113*, 2359−2369.
(10) Vankoppen, P. A. M.; Bowers, M. T.; Fisher, E. R.; Armentrout, P. B. *J. Am. Chem. Soc.* **1994**, *116*, 3780−3791.
(11) Davidson, E. R. *Chem. Rev.* **2000**, *100*, 351−352.
(12) Eller, K.; Schwarz, H. *Chem. Rev.* **1991**, *91*, 1121−1177.
(13) Torrent, M.; Sola, M.; Frenking, G. *Chem. Rev.* **2000**, *100*, 439−493.
(14) Ziegler, T. *J. Chem. Soc., Dalton Trans.* **2002**, 642−652.
(15) Armentrout, P. B. *Science* **1991**, *251*, 175−179.
(16) Yarkony, D. R. *J. Phys. Chem.* **1996**, *100*, 18612−18628.
(17) Plattner, D. *Angew. Chem., Int. Ed.* **1999**, *38*, 82−86.

10.1021/om0342098 CCC: $27.50
Publication on Web 01/20/2004

reaction has been emphasized by Schröder, Shaik, and Schwarz[18] and Poli and Harvey[19] in two recent reviews of two-state reactivity and spin-forbidden chemical reactions in organometallic chemical reaction pathways, respectively. In principle, the reaction rate can be limited by the transition structure (TS) on the PES for either electronic state or by the rate of crossing between surfaces. Therefore, it is necessary to locate and characterize the stationary points on each PES and the key regions of the PESs where the relevant spin states lie close in energy and geometry, corresponding to the crossing points (CPs). Computational methods of theoretical chemistry are suitable tools for the study of this type of phenomenon, and several authors have addressed this complex and demanding research area.[3,19−56]

As pointed out by Shaik, Schwarz, et al.,[57] the two-state reactivity can be traced back to the electronic structure of MO^+ cations (M = Cr−Cu);[58,59] these cations can be the result of an oxidation process involving the correspoding metal dioxide cation counterpart, MO_2^+. Gas-phase reactivities of some metal dioxide cations have been studied by different research groups as well as the oxidation reactions initiated by these metal-dioxo species.[60−73] In particular, reactions between hydrocarbons and vanadium oxides are important to many industrial processes that stimulate research in this field[7,74−77]. From the experimental side, well-controlled studies on relative small vanadium oxide clusters not only provide a new avenue to obtain detailed information on structures and interactions between oxygen and vanadium atoms but also provide models for the chemical reactions involving vanadium oxide materials and vanadium oxide surfaces[78,79]

A. W. Castleman Jr. and co-workers have studied, by means of an ion beam mass spectrometer coupled with a laser vaporization source, the reactions of vanadium oxide clusters of different stoichiometries, $V_xO_y^+$, with various compounds such as C_2H_4, C_2H_6, C_2F_6, CH_3CF_3, CCl_4, and CH_2F_2, due to the recognition of the important role they play in many reactive processes.[80−88] Schwarz et al. have selected Fourier transform mass spectrom-

(18) Schröder, D.; Schwarz, H.; Shaik, S. In *Metal-Oxo and Metal-Peroxo Species in Catalytic Oxidations*; Meunier, B., Ed.; Springer-Verlag: Berlin, 2000; pp 91−123.
(19) Poli, R.; Harvey, J. N. *Chem. Soc. Rev.* **2003**, *32*, 1−8.
(20) Koga, N.; Morokuma, K. *Chem. Phys. Lett.* **1985**, *119*, 371−374.
(21) Manaa, M. R.; Yarkony, D. R. *J. Chem. Phys.* **1991**, *95*, 1808−1816.
(22) Farazdel, A.; Dupuis, M. *J. Comput. Chem.* **1991**, *12*, 276−282.
(23) Jensen, F. *J. Am. Chem. Soc.* **1992**, *114*, 1596−1603.
(24) Yarkony, D. R. *J. Phys. Chem.* **1993**, *97*, 4407−4412.
(25) Nguyen, K. A.; Gordon, M. S.; Montgomery, J. A.; Michels, H. H.; Yarkony, D. R. *J. Chem. Phys.* **1993**, *98*, 3845−3849.
(26) Chang, A. H. H.; Yarkony, D. R. *J. Chem. Phys.* **1993**, *99*, 6824−6831.
(27) Bearpark, M. J.; Robb, M. A.; Schlegel, H. B. *Chem. Phys. Lett.* **1994**, *223*, 269−274.
(28) Dunn, K. M.; Morokuma, K. *J. Phys. Chem.* **1996**, *100*, 123−129.
(29) Anglada, J. M.; Bofill, J. M.; Olivella, S.; Sole, A. *J. Am. Chem. Soc.* **1996**, *118*, 4636−4647.
(30) Musaev, D. G.; Morokuma, K. *J. Phys. Chem.* **1996**, *100*, 11600−11609.
(31) Danovich, D.; Shaik, S. *J. Am. Chem. Soc.* **1997**, *119*, 1773−1786.
(32) Cui, Q.; Morokuma, K. *Chem. Phys. Lett.* **1997**, *272*, 319−327.
(33) Sadygov, R. G.; Yarkony, D. R. *J. Chem. Phys.* **1997**, *107*, 4994−4999.
(34) Anglada, J. M.; Bofill, J. M. *J. Comput. Chem.* **1997**, *18*, 992−1003.
(35) Aschi, M.; Harvey, J. N.; Schalley, C. A.; Schröder, D.; Schwarz, H. *Chem. Commun.* **1998**, 531−532.
(36) Schröder, D.; Heinemann, C.; Schwarz, H.; Harvey, J. N.; Dua, S.; Blanksby, S. J.; Bowie, J. H. *Chem. Eur. J.* **1998**, *4*, 2550−2557.
(37) Schalley, C. A.; Harvey, J. N.; Schröder, D.; Schwarz, H. *J. Phys. Chem. A* **1998**, *102*, 1021−1035.
(38) Harvey, J. N.; Aschi, M.; Schwarz, H.; Koch, W. *Theor. Chem. Acc.* **1998**, *99*, 95−99 (http://www.bris.ac.uk/Depts/Chemistry/staff/jharvey.htm).
(39) Stevens, J. E.; Cui, Q.; Morokuma, K. *J. Chem. Phys.* **1998**, *108*, 1452−1458.
(40) Kaledin, A. L.; Cui, Q.; Heaven, M. C.; Morokuma, K. *J. Chem. Phys.* **1999**, *111*, 5004−5016.
(41) Wilsey, S.; Bernardi, F.; Olivucci, M.; Robb, M. A.; Murphy, S.; Adam, W. *J. Phys. Chem. A* **1999**, *103*, 1669−1677.
(42) Yoshizawa, K.; Shiota, Y.; Yamabe, T. *J. Chem. Phys.* **1999**, *111*, 538−545.
(43) Yoshizawa, K.; Shiota, Y.; Yamabe, T. *J. Am. Chem. Soc.* **1999**, *121*, 147.
(44) Aschi, M.; Harvey, J. N. *J. Chem. Soc., Perkin Trans. 2* **1999**, 1059−1062.
(45) Barrientos, C.; Redondo, P.; Largo, A. *Chem. Phys. Lett.* **1999**, *306*, 168−178.
(46) Aschi, M.; Grandinetti, F. *Int. J. Mass Spectrom.* **2000**, *201*, 151−160.
(47) Oiestad, E. L.; Harvey, J. N.; Uggerud, E. *J. Phys. Chem. A* **2000**, *104*, 8382−8388.
(48) Smith, K. M.; Poli, R.; Harvey, J. N. *New J. Chem.* **2000**, *24*, 77−80.
(49) Harvey, J. N. *J. Am. Chem. Soc.* **2000**, *122*, 12401−12402.
(50) Harvey, N. H. In *Computational Organometallic Chemistry*; Cundari, T. R., Ed.; Marcel Deker, Inc.: New York, 2000; pp 291−321.
(51) Smith, K. M.; Poli, R.; Harvey, J. N. *Chem. Eur. J.* **2001**, *7*, 1679−1690.
(52) Ijjaali, F.; El-Mouhtadi, M.; Esseffar, M.; Alcami, M.; Mo, O.; Yanez, M. *Phys. Chem. Chem. Phys.* **2001**, *3*, 179−183.
(53) Aschi, M.; Largo, A. *Chem. Phys.* **2001**, *265*, 251−261.
(54) Le Grognec, E.; Poli, R. *Chem. Eur. J.* **2001**, *7*, 4572−4583.
(55) Hess, J. S.; Leelasubcharoen, S.; Rheingold, A. L.; Doren, D. J.; Theopold, K. H. *J. Am. Chem. Soc.* **2002**, *124*, 2454−2455.
(56) Green, J. C.; Harvey, J. N.; Poli, R. *J. Chem. Soc., Dalton Trans.* **2002**, 1861−1866.
(57) Shaik, S.; Danovich, D.; Fiedler, A.; Schröder, D.; Schwarz, H. *Helv. Chim. Acta* **1995**, *78*, 1393.
(58) Carter, E. A.; Goddard, W. A. *J. Phys. Chem.* **1988**, *92*, 5679−5683.
(59) Fiedler, A.; Schröder, D.; Shaik, S.; Schwarz, H. *J. Am. Chem. Soc.* **1994**, *116*, 10734−10741.
(60) Irikura, K. K.; Beauchamp, J. L. *J. Am. Chem. Soc.* **1989**, *111*, 75−85.
(61) Cassady, C. J.; McElvany, S. W. *Organometallics* **1992**, *11*, 2367−2377.
(62) Pope, R. M.; Vanorden, S. L.; Cooper, B. T.; Buckner, S. W. *Organometallics* **1992**, *11*, 2001−2003.
(63) Pope, R. M.; Buckner, S. W. *Organic Mass Spectrom.* **1993**, *28*, 1616−1622.
(64) Schröder, D.; Fiedler, A.; Schwarz, J.; Schwarz, H. *Inorg. Chem.* **1994**, *33*, 5094−5100.
(65) Wesendrup, R.; Schwarz, H. *Angew. Chem., Int. Ed. Engl.* **1995**, *34*, 2033−2035.
(66) Fiedler, A.; Kretzschmar, I.; Schröder, D.; Schwarz, H. *J. Am. Chem. Soc.* **1996**, *118*, 9941−9952.
(67) Heinemann, C.; Cornehl, H. H.; Schröder, D.; Dolg, M.; Schwarz, H. *In. Chem.* **1996**, *35*, 2463−2475.
(68) Kretzschmar, I.; Schröder, D.; Schwarz, H. *Int. J. Mass Spectrom.* **1997**, *167*, 103−115.
(69) Kretzschmar, I.; Fiedler, A.; Harvey, J. N.; Schröder, D.; Schwarz, H. *J. Phys. Chem. A* **1997**, *101*, 6252−6264.
(70) Cornehl, H. H.; Wesendrup, R.; Diefenbach, M.; Schwarz, H. *Chem.-A Eur. J.* **1997**, *3*, 1083−1090.
(71) Shilov, A. E.; Shul'pin, G. B. *Chem. Rev.* **1997**, *97*, 2879−2932.
(72) Shilov, A. E.; Shteinman, A. *Acc. Chem. Res.* **1999**, *32*, 763−771.
(73) Shiota, Y.; Yoshizawa, K. *J. Am. Chem. Soc.* **2000**, *122*, 12317−12326.
(74) Escribano, V. S.; Busca, G.; Lorenzelli, V. *J. Phys. Chem.* **1990**, *94*, 8945−8950.
(75) Oyama, S. T.; Somorjai, G. A. *J. Phys. Chem.* **1990**, *94*, 5022−5028.
(76) Ruth, K.; Kieffer, R.; Burch, R. *J. Catal.* **1998**, *175*, 16−26.
(77) Linke, D.; Wolf, D.; Baerns, M.; Timpe, O.; Schlogl, R.; Zeyss, S.; Dingerdissen, U. *J. Catal.* **2002**, *205*, 16−31.
(78) Vyboishchikov, S. F.; Sauer, J. *J. Phys. Chem. A* **2000**, *104*, 10913−10922.
(79) Vyboishchikov, S. F.; Sauer, J. *J. Phys. Chem. A* **2001**, *105*, 8588−8598.
(80) Bell, R. C.; Zemski, K. A.; Kerns, K. P.; Deng, H. T.; Castleman, A. W., Jr. *J. Phys. Chem. A* **1998**, *102*, 1733−1742.

etry to study the gas-phase reactivity of metal dioxide cation MO_2^+ (M = Ti, V, Zr, and Nb) toward simple hydrocarbons, while calculations have been carried out to obtain electronic and thermochemical properties of the reactivity pattern.[89] Fielicke and Rademann have investigated the interaction of $V_xO_y^+$ clusters with alkenes and alkanes and their relationship with the corresponding chemical reactivity.[90] These works provide new insight into the structure and bonding of vanadium-containing compounds.

Gas-phase vanadium oxide clusters have been previously examined theoretically[78,79,89,91−93] as well as experimentally.[89,94,95] We have an ongoing interest in exploring how the associated spin state affects the chemical reactivity of simple metal oxides, and a recent study on the reaction between VO_2^+ and C_2H_4 has been published.[96] Following the methodology of this previous study, in this work we report the first complete study of the title reaction of vanadyl cation, VO_2^+, with ethane, C_2H_6, to yield $V(OH)_2^+ + C_2H_4$ and/or $VO^+ + H_2O + C_2H_4$ as a good example of a chemical process involving singlet and triplet electronic states. Therefore, we have characterized the corresponding stationary points and the crossing point between both surfaces. In addition, we have performed a comparative analysis among the results obtained in the previous work on the oxidation of ethene[96] and propane[97] by VO_2^+ and the present results, to explain the different reactivity patterns.

Another important goal of this work is to analyze the tautomerization process between hydrated vanadium oxide, $VO(H_2O)^+$, and vanadium dihydroxide, $V(OH)_2^+$, cations, either in the gas phase or catalyzed by a water molecule, and this work reports the role of solvation by water on this rearrangement.

This paper is divided in three sections. Methods and computational strategy are described in section 2. Section 3 contains the main results and discussions. The final conclusions that arise from the current research are summarized in section 4.

2. Methods and Computational Strategy

All computations are carried out using the GAUSSIAN98 program package.[98] The calculations were performed at first approximation at the unrestricted or restricted B3LYP level,[99,100] using the standard all-electron 6-311G(2d,p)[101] basis sets implemented in GAUSSIAN98. We adopted this level and basis set because it was used to calculate the activation energy of the similar reaction $VO_2^+ + C_2H_4$, as well as in previous works with complex systems involving vanadium oxide systems,[91−93] and they yielded satisfactory results. Therefore, we are confident with the data calculated at this computing level for this type of reaction. The present calculations are computationally taxed, but for the sake of completeness, single-point CCSD/6-311G(2d,p)//B3LYP/6-311G(2d,p) calculations are performed at selected structures.

The Berny algorithm has been employed for the geometry optimizations[102] without constraint, and the computed stationary points have been characterized as minima or transition states by diagonalizing the Hessian matrix and analyzing the vibrational normal modes (transition vector).[102] The intrinsic reaction coordinate method (IRC)[104,105] has been used to describe minimum energy paths from TSs to the corresponding minima. The activation parameters were calculated assuming ideal gas behavior from the harmonic frequencies and moments of inertia by standard methods,[106] at 298.15 K.

All coordinates were optimized in searches for the CP between the two PESs in which DFT energies and gradients were calculated for each spin multiplicity. Starting from the TS closest to the crossing seams, the reaction pathway was traced down to the corresponding minimum. Thereafter, each optimized point along the IRC path was submitted to a single-point energy calculation with the other electronic state. In this way, we obtain the CP as the structures that have identical geometry and energy in the singlet and triplet states. For the sake of comparison, the mathematical algorithm to obtain minimum energy crossing points (MECPs) proposed by Harvey et al.[38] have been also employed. The CP that we obtain in this way can be considered as estimates of the MECPs between singlet and triplet hypersurfaces. The natural population analysis has been made by using the natural bond orbital (NBO)[107,108] option as implemented in GAUSSIAN98.

(81) Bell, R. C.; Zemski, K. A.; Castleman Jr, A. W. *J. Phys. Chem. A* **1998**, *102*, 8293−8299.
(82) Bell, R. C.; Zemski, K. A.; Castleman, A. W., Jr. *J. Phys. Chem. A* **1999**, *103*, 1585−1591.
(83) Bell, R. C.; Zemski, K. A.; Castleman, A. W., Jr. *J. Phys. Chem. A* **1999**, *103*, 2992.
(84) Kooi, S. E.; Castleman Jr, A. W. *J. Phys. Chem. A* **1999**, *103*, 5671−5674.
(85) Bell, R. C.; Zemski, K. A.; Castleman, A. W. *J. Cluster Sci.* **1999**, *10*, 509−524.
(86) Zemski, K. A.; Justes, D. R.; Castleman, A. W. *J. Phys. Chem. B* **2002**, *106*, 6136−6148.
(87) Bell, R. C.; Zemski, K. A.; Justes, D. R.; Castleman, A. W. *J. Chem. Phys.* **2001**, *114*, 798−811.
(88) Zemski, K. A.; Justes, D. R.; Castleman, A. W. *J. Phys. Chem. A* **2001**, *105*, 10237−10245.
(89) Harvey, J. N.; Aschi, M. *Phys. Chem. Chem. Phys.* **1999**, *1*, 5555−5563.
(90) Fielicke, A.; Rademann, K. *Phys. Chem. Chem. Phys.* **2002**, *4*, 2621−2628.
(91) Calatayud, M.; Andrés, J.; Beltrán, A.; Silvi, B. *Theor. Chem. Acc.* **2001**, *105*, 299−308.
(92) Calatayud, M.; Silvi, B.; Andrés, J.; Beltrán, A. *Chem. Phys. Lett.* **2001**, *333*, 493−503.
(93) Calatayud, M.; Andrés, J.; Beltrán, A. *J. Phys. Chem. A* **2001**, *105*, 9760−9775.
(94) Foltin, M.; Stueber, G. J.; Bernstein, E. R. *J. Chem. Phys.* **1999**, *111*, 9577−9586.
(95) Asmis, K. R.; Brummer, M.; Kaposta, C.; Santambrogio, G.; von Helden, G.; Meijer, G.; Rademann, K.; Woste, L. *Phys. Chem. Chem. Phys.* **2002**, *4*, 1101−1104.
(96) Gracia, L.; Sambrano, J. R.; Safont, V. S.; Calatayud, M.; Beltrán, A.; Andres, J. *J. Phys. Chem. A* **2003**, *107*, 3107−3120.
(97) Engeser, M.; Schlangen, M,; Schröder, D.; Schwarz, H. *Organometallics* **2003**, *22*, 3933−3943.
(98) Frisch, M. J.; Trucks, G. W.; Schlegel, H. B.; Scuseria, G. E.; Robb, M. A.; Cheeseman, J. R.; Zakrzewski, V. G.; Montgomery, J. A.; Stratmann, R. E.; Burant, J. C.; Dapprich, S.; Millam, J. M.; Daniels, A. D.; Kudin, K. N.; Strain, M. C.; Farkas, O.; Tomasi, J.; Barone, V.; Cossi, M.; Cammi, R.; Mennucci, B.; Pomelli, C.; Adamo, C.; Clifford, S.; Ochterski, J.; Petersson, G. A.; Ayala, P. Y.; Cui, Q.; Morokuma, K.; Malick, D. K.; Rabuck, A. D.; Raghavachari, K.; Foresman, J. B.; Cioslowski, J.; Ortiz, J. V.; Stefanov, B. B.; Liu, G.; Liashenko, A.; Piskorz, P.; Komaromi, I.; Gomperts, R.; Martin, R. L.; Fox, D. J.; Keith, T.; Al-Laham, M. A.; Peng, C. Y.; Nanayakkara, A.; Gonzalez, C.; Challacombe, M.; Gill, P. M. W.; Johnson, B. G.; Chen, W.; Wong, M. W.; Andres, J. L.; Head-Gordon, M.; Replogle, E. S.; Pople, J. A. *Gaussian98 (Revision A.1)*; Gaussian, Inc.: Pittsburgh, PA, 1998.
(99) Lee, C.; Yang, R. G.; Parr, R. G. *Phys. Rev. B* **1988**, *37*, 785−789.
(100) Becke, A. D. *J. Chem. Phys.* **1993**, *98*, 5648−5652.
(101) Pople, J. A.; Head-Gordon, M.; Raghavachari, K. *J. Chem. Phys.* **1987**, *87*, 5968.
(102) Schlegel, H. B. *J. Comput. Chem.* **1982**, *3*, 214−218.
(103) McIver, J. W., Jr. *Acc. Chem. Res.* **1974**, *7*, 72−77.
(104) Fukui, K. *J. Phys. Chem.* **1970**, *74*, 4161−4163.
(105) González, C.; Schlegel, H. B. *J. Chem. Phys.* **1989**, *90*, 2154−2161.
(106) González, C.; Schlegel, H. B. *J. Phys. Chem.* **1990**, *94*, 5523−5527.
(107) Reed, A. E.; Weinstock, R. B.; Weinhold, F. *J. Chem. Phys.* **1985**, *83*, 735−746.
(108) Reed, A. E.; Curtiss, L. A.; Weinhold, F. *Chem. Rev.* **1988**, *88*, 899−926.

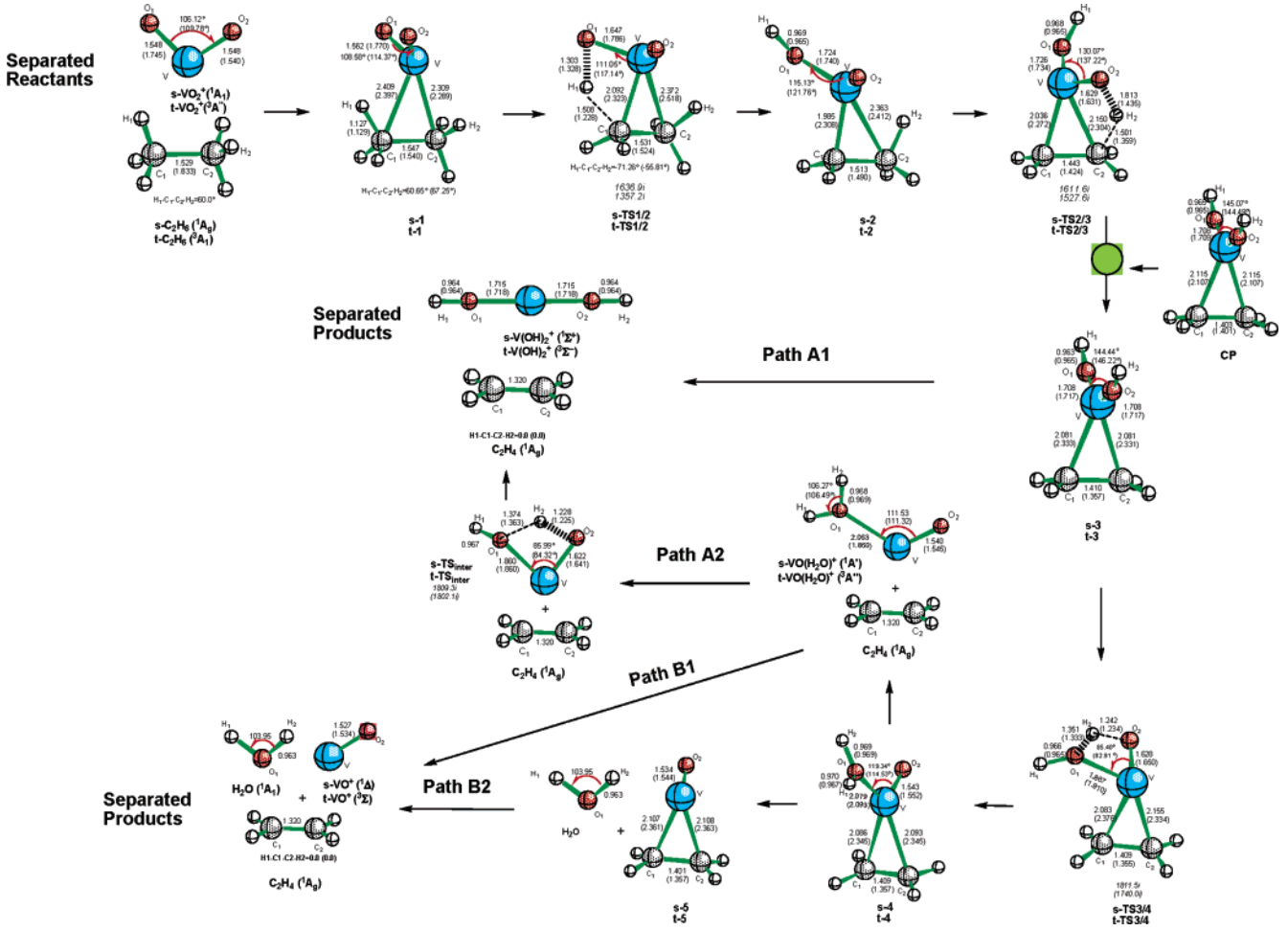

Figure 1. Structures (distances in Å and angles in deg) of the stationary points found in the first singlet state and first triplet electronic states (in brackets) and structure of the crossing point, **CP**, found between **s-TS2/3** and **s-3** (in parentheses are presented corresponding values using the algorithm proposed by Harvey et al.[38] to characterize the MECP) at the B3LYP/6-311G(2d,p) level. For the TSs the imaginary vibrational frequencies (cm^{-1}) are shown in italics.

3. Results and Discussion

The geometries of the stationary points at both singlet (s) and triplet (t) electronic states are depicted in Figure 1 and the Gibbs free energy profiles in Figure 2. An analysis of these figures points out that the reactivity patterns of the s and t spin states are rather similar. Two combinations are possible for the reactants and products, depending on its particular electronic state. The most stable combination of reactants is formed by **s-VO_2^+** ($^1A_1$) and C_2H_6 (^1A_g), thus belonging to the overall singlet PES. The triplet state combination, **t-VO_2^+** ($^3A''$) + C_2H_6 (^1A_g), stands 35.6 kcal/mol above the singlet. For the products, four exit channels can be proposed, following the order of stability: **t-$V(OH)_2^+$** ($^3\Sigma^-$) + C_2H_4 (^1A_g), −30.0 kcal/mol, **s-$V(OH)_2^+$** ($^1\Sigma^+$) + C_2H_4 (^1A_g), −6.2 kcal/mol, **t-VO^+** ($^3\Sigma$) + H_2O ($^1A_1$) + C_2H_4 (^1A_g), 9.3 kcal/mol, and **s-VO^+** ($^1\Delta$) + H_2O ($^1A_1$) + C_2H_4 (^1A_g), 35.8 kcal/mol. Then, it is obvious that from the most stable reactants, **s-VO_2^+** and C_2H_6, to the most stable products, **t-$V(OH)_2^+$** and C_2H_4, at least one intersystem crossing must take place.

3.1. Formation of $V(OH)_2^+ + C_2H_4$ Products. The first stage of the reaction in both electronic states corresponds to the approach and interaction of vanadyl cation VO_2^+ toward the ethane fragment, with formation of the corresponding complexes, **s-1** and **t-1**, for the s and t electronic states, respectively; a noticeable electronic charge transfer takes place from the ethane moiety to the vanadyl cation, 0.21 and 0.19 au at **s-1** and **t-1**, respectively. These values point out that these ion−molecule complexes appear to be mostly electrostatic in nature, and no geometrical perturbation at either fragment is sensed. Therefore, the initial step is the formation of a very stable association complex between V and both C atoms, a three-membered ring, without an activation barrier to overcome. Any attempt to localize on the potential energy surface (singlet and triplet) an ion complex formed by the interaction of the oxygen atom of the VO_2^+ moiety with C_2H_6 has been unsuccessful.

The next step is associated with a hydrogen transfer between C_1 and O atoms to yield the **s-2** (**t-2**) intermediate, via the transition structure **s-TS1/2** (**t-TS1/2**). The activation free energy is 25.8 and 14.2 kcal/mol, respectively, while the formation of **s-2** (**t-2**) is quite exothermic, 18.4 and 32.2 kcal/mol, respectively. These intermediates correspond to an O-protonated ethyl vanadium oxide.[109,110] The channel from **s-2** (**t-2**) to **s-3** (**t-3**) takes place along **s-TS2/3** (**t-TS2/3**), associated with another

(109) Bottomley, F.; Sutin, L. *Adv. Organomet. Chem.* **1988**, *28*, 339−396.
(110) Harvey, J. N.; Diefenbach, M.; Schröder, D.; Schwarz, H. *Int. J. Mass Spectrom.* **1999**, *182/183*, 85−97.

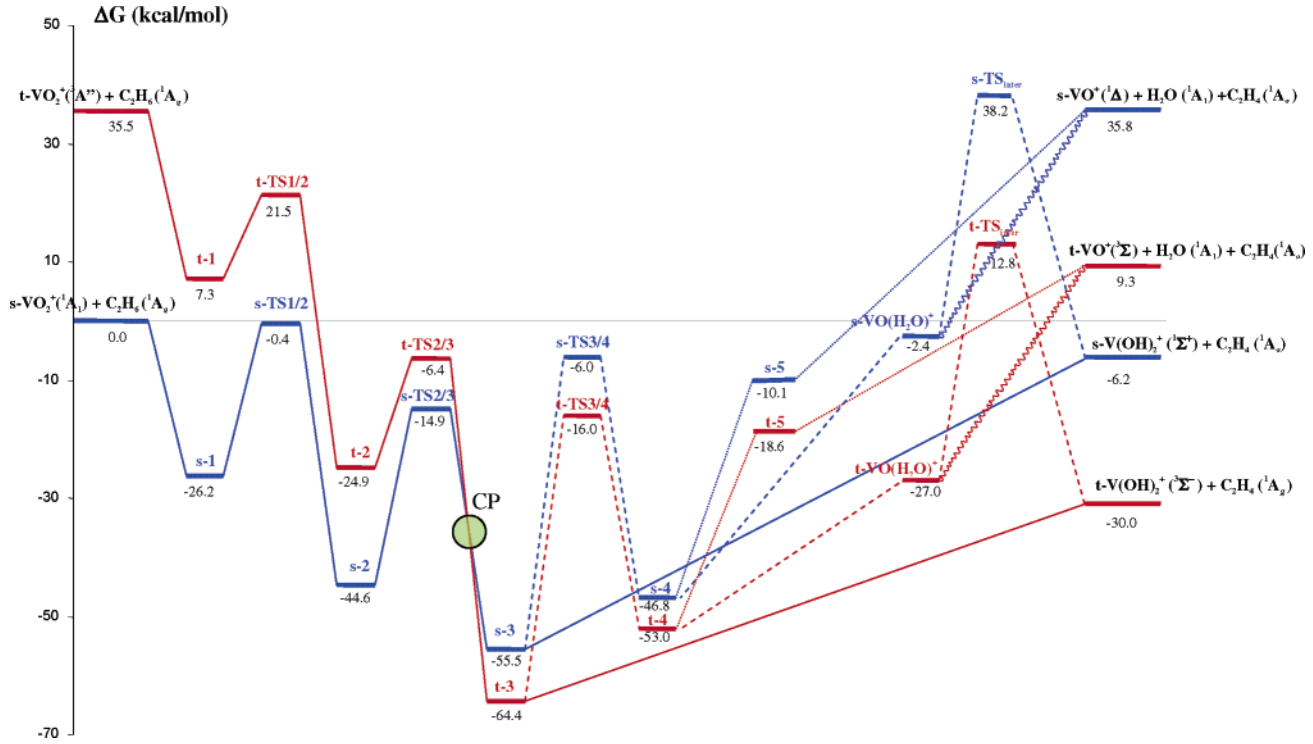

Figure 2. Gibbs free energy profiles at 298.15 K, relative to the reactants in the singlet state, for the singlet (in blue) and triplet (in red) states at the B3LYP/6-311G(2d,p) level. Δ*G* values (kcal/mol) are indicated.

migration of the hydrogen atom bonded from C_2 to the O atom, i.e., a β-hydrogen transfer from the alkyl group to the oxo moiety. Therefore, these TSs are associated with an activation of C−H bonds of ethane, and they can be considered as consecutive hydrogen transfer processes (the hydrogen atoms being transferred, H_1 and H_2, are positively charged, in the range 0.31−0.39 au) and present larger and similar values of imaginary vibrational frequencies, around 1600i cm^{-1} at **s-TS1/2** (**s-TS2/3**) and in the range 1350−1530i cm^{-1} at **t-TS1/2** (**t-TS2/3**). An analysis of the geometry shows that these TSs are four-membered rings.

The intersystem crossing, via **CP**, between the singlet and triplet PESs occurs during the path connecting **s-TS2/3** (**t-TS2/3**) with the very stable intermediates **s-3** (**t-3**). The existence of this **CP** opens the possibility for an intersystem crossing to take place. The geometry of the **CP** is depicted in Figure 1. An analysis of the corresponding values shows that **CP** is geometrically and energetically closer to **s-3** than to **t-3**. The $V-C_1$/$V-C_2$ distance is 2.081 Å (2.331 Å) in **s-3** (**t-3**) and 2.115 Å in **CP**. Also, the O_1-V-O_2 bond angle in **CP** is 145.07°, compared to 144.44° in **s-3** and 146.22° in **t-3**. Accordingly, the energy of **CP** is ca. 0.2 and 7.8 kcal/mol over **s-3** and **t-3**, respectively. For comparison purposes, we have also used the algorithm proposed by Harvey et al.[38] to characterize the MECP, and the corresponding geometrical values are also presented in Figure 1. It is important to note that similar values of the geometrical parameters and relative energies are found (total energy values of the **CP** and the MECP are −1174.138353 and −1774.138432 hartrees at the B3LYP/6-311G(2d,p) level, respectively).

The **s-TS2/3** is 8.5 kcal/mol more stable than **t-TS2/3**. The initial C−H activation involves a singlet electronic state, while the second C−H activation takes place in both s and t electronic states. From **CP** the reactive channel taking place in the t state is energetically favorable. The intermediates, **s-3** and **t-3**, are the most stable minima on the PES, −55.5 and −64.4 kcal/mol, respectively, suggesting that they are long-lived species and they can be considered as product complexes between the dihydroxide cation and ethene fragment. A small value of the negative charge is transferred from the ethene moiety to the dihydroxide fragment, 0.02 and 0.10 au, respectively. In fact, at **CP**, the positive charge of the $V(OH_2)^+$ fragment is 0.91 au. Therefore, **s-3** and **t-3** can be connected with the separated products, **s-V(OH)$_2^+$** + C_2H_4 and **t-V(OH)$_2^+$** + C_2H_4, respectively, climbing up a barrier height of 49.3 and 34.4 kcal/mol. The formation of **s-V(OH)$_2^+$** and **t-V(OH)$_2^+$** is exergonic, and the dissociation limit of both processes lies 6.2 and 30.0 kcal/mol below the entrance channel, respectively.

From these results, the most thermodinamically and kinetically favorable products are obtained along a dehydrogenation of the ethane to yield ethene and vanadium dihydroxide cation; this result is in agreement with experimental data.[110] If the spin inversion is easy, it is conceivable that a mechanistic path, starting from the reactants in the singlet state, **s-VO$_2^+$** + C_2H_6, goes through **s-1**, **s-TS1/2**, **s-2**, and **s-TS2/3**; then **CP** is found, and a downhill path can be taken on the triplet state PES to render the most stable intermediate, **t-3**. Finally, the most stable product outcome is reached: **t-V(OH)$_2^+$** + C_2H_4, path A1. This channel is the most energetically favorable, and it appears as an inverted energy profile. All stationary points lie below the dissociation limit of the entrance channel, **s-VO$_2^+$** + C_2H_6, **s-TS1/2** being the higher stationary point along the reaction pathway (see Figure 2). The **CP** between s and t electronic states takes place after the transition states (both singlet and triplet), associated with the most energetically demanding barriers. The initial steps, C−H activation processes via

TS1/2 and **TS2/3**, exclusively involve the singlet surface, but to obtain the global minimum in the VO_2^+/ethane system on the triplet surface, the **CP** is necessary. Therefore, the switch between spin states controls the outcome of the reaction between VO_2^+ and ethane.

From intermediates, **s-3** and **t-3**, the reaction may continue toward formation of different products. Therefore, both minima can be considered branching points opening up two different reaction channels. **s-3** (**t-3**) can yield **s-4** (**t-4**), via **s-TS3/4** (**t-TS3/4**), associated with an intramolecular hydrogen transfer between O_2 and O_1. Both **TS3/4** present values of imaginary vibrational frequencies in the range 1740i−1811i cm^{-1}, and the positive charge of the transferred hydrogen at both TSs is around 0.51 au. **s-4** and **t-4** intermediates can be considered encounter complexes. Therefore, from **s-4** or **t-4**, ethene and the corresponding hydrated oxide cations, **s-VO(H$_2$O)$^+$** or **t-VO(H$_2$O)$^+$**, are obtained. The geometry of the water ligand in **s-4/t-4** and **s-VO(H$_2$O)$^+$/t-VO(H$_2$O)$^+$** is almost undisturbed compared to the free H_2O, indicating that the interaction is predominantly electrostatic. From **s-4** and **t-4**, the interconversion of the hydrated oxide cation, $VO(H_2O)^+$, to the dihydroxide cation, $V(OH)_2^+$, along **s-TS$_{inter}$/t-TS$_{inter}$** is possible, associated with a 1,3-H shift from the oxygen atom of the water fragment, O_1, to the oxygen, O_2, to yield the corresponding dihydroxide cation **s-V(OH)$_2^+$** and **t-V(OH)$_2^+$**, respectively. Energetically, **s-TS$_{inter}$** is 25.4 kcal/mol higher in energy than **t-TS$_{inter}$**, both TSs also present values of imaginary vibrational frequencies around 1800i cm^{-1}, and the positive charge of the transferred hydrogen at both TSs is 0.50 au.

A comparison of the stability of the dihydroxide cation, **t-VO(H$_2$O)$^+$**, and the corresponding hydrated oxide cation, **t-V(OH)$_2^+$**, reveals that the formation of the first ones is more stable (3 kcal/mol) than the latter, in agreement with previous work of Koyanagi et al.[111] (11.7 kcal/mol) and Ricca and Bauschlicher.[112] Furthermore, in these systems, the formation of O−H bonds with the oxygen atoms is preferred over the presence of an intact water molecule. The barrier height associated with the 1,3-hydrogen migration is substantial, 39.8 kcal/mol, in agreement with the value reported by Koyanagi et al.[111] (40.6 kcal/mol). It is also important to compare the relative energies of **s/t-TS$_{inter}$** and **s/t-TS3/4**, both associated with 1,3-hydrogen migration in the isolated vanadyl cation framework and in the presence of the ethene fragment, respectively. An analysis of the results of Figure 2 reveals that the second is more stable than the first and the corresponding values of the barrier heights are in the ranges 39.8−40.6 and 48.4−49.5 kcal/mol, respectively. The presence of the ethene moiety in the latter increases the barrier height, around 9.0 kcal/mol, with respect to the **s/t-TS$_{inter}$**. Both TSs, **s/t-TS3/4** and **s/t-TS$_{inter}$**, are cyclic structures. **s/t-TS3/4** are four-membered rings, while **s/t-TS$_{inter}$** are composed of a four-membered ring linked across the V atom to a three-membered ring, corresponding with the C_1-V-C_2 moiety.

We can then trace two reaction channels that connect the most stable reactants **s-VO$_2^+$** + C_2H_6 with the products **t-V(OH)$_2^+$** + C_2H_4, via **s-1**, **s-TS1/2**, **s-2**, **s-TS2/3**, **CP**, and **t-3** (path A1) or via **s-1**, **s-TS1/2**, **s-2**, **s-TS2/3**, **CP**, **t-3**, **t-TS3/4**, **t-4**, **t-VO(H$_2$O)$^+$**, and **t-TS$_{inter}$** (path A2). The reaction pathway along A1 is more simple and energetically favorable than A2, and it is in nice agreement with the experimental data that reports that VO_2^+ reacts with ethane to yield exclusively the **t-V(OH)$_2^+$** cation and ethene.[89,111] In addition, the localization of the **CP** points out that the switch between singlet and triplet spin states should determine that the product outcome due to **CP** takes place after the **s-TS1/2** and before the branching point, **t-3**.

3.2. Rearrarangement between the Hydrated Vanadium Oxide, VO(H$_2$O)$^+$, and Vanadium Dihydroxide, V(OH)$_2^+$. The Role of a Water Molecule. From previous experimental works,[111,113] the active participation of a water molecule in the tautomerization between the hydrated vanadium oxide, $VO(H_2O)^+$, and vanadium dihydroxide, $V(OH)_2^+$, associated with a 1,3-hydrogen migration, has been proposed. These experimental data point out that the presence of water can decrease the energy barrier significantly via a proton-shuttle mechanism.[111] However, to our knowledge no theoretical studies have been published on the catalysis by water molecules in these systems. The geometries and the free energy profiles of the stationary points from **s-3/t-3** to the corresponding products in the presence of a discrete water molecule are shown in Figures 3 and 4, respectively. It can be observed that the presence of a water molecule leads to four intermediates: the hydrated **s-3w/t-3w**, **s-4w/t-4w**, **s-VO(H$_2$O)$^+$w/t-VO(H$_2$O)$^+$w**, and **s-V(OH)$_2^+$w/t-V(OH)$_2^+$w**. In these intermediates, the water molecule is mainly interacting with the OH group of both hydrated and dihydroxide fragments as proton acceptor, and the values of stabilization free energy due to these additional H-bonds are in the range 6.3−16.6 and 9.4−14.5 kcal/mol for singlet and triplet, respectively. However, the activation free energies of the corresponding TSs, **s-TS3/4w** (**t-TS3/4w**) and **s-TS$_{inter}$w** (**t-TS$_{inter}$w**), computed with respect to the corresponding minima, are 18.2 (20.2) and 11.1 (13.6) kcal/mol, respectively, significantly smaller than those of the uncatalyzed process: 49.5 (48.4) and 40.6 (39.8) kcal/mol, respectively. The catalysis of such tautomeric processes by a water molecule can be attributed to a smaller distortion of the OVO fragment in the transition structures, **s-TS3/s-4w** (**t-TS3/t-4w**) and **s-TS$_{inter}$w** (**t-TS$_{inter}$w**). For example, in the uncatalyzed process the OVO angle suffers a larger distortion during the process than in the presence of a water molecule. Moreover, the geometry of these TSs in this water-assisted system shows that the water molecule interacts with the O−H fragment as proton acceptor and with the oxygen atom as a proton donor. In these stationary points, there are a short (in the range 1.386−1.500 Å) and a large (in the range 1.688−1.820 Å) H-bond that contribute to stabilize the TSs. Population analysis indicates that the proton transfer character is increased in the solvated complex compared to the isolated system. In particular, the charge of the distorted H_3O in **t-TS3/4w** and **t-TS$_{inter}$w** is 0.78 and 0.76 au, respectively,

(111) Koyanagi, G. K.; Bohme, D. K.; Kretzschmar, I.; Schröder, D.; Schwarz, H. *J. Phys. Chem. A* **2001**, *105*, 4259−4271.
(112) Ricca, A.; Bauschlicher, C. W. *J. Phys. Chem. A* **1997**, *101*, 8949−8955.
(113) Bohme, D. K. *Int. J. Mass Spectrom. Ion Processes* **1992**, *115*, 95−110.

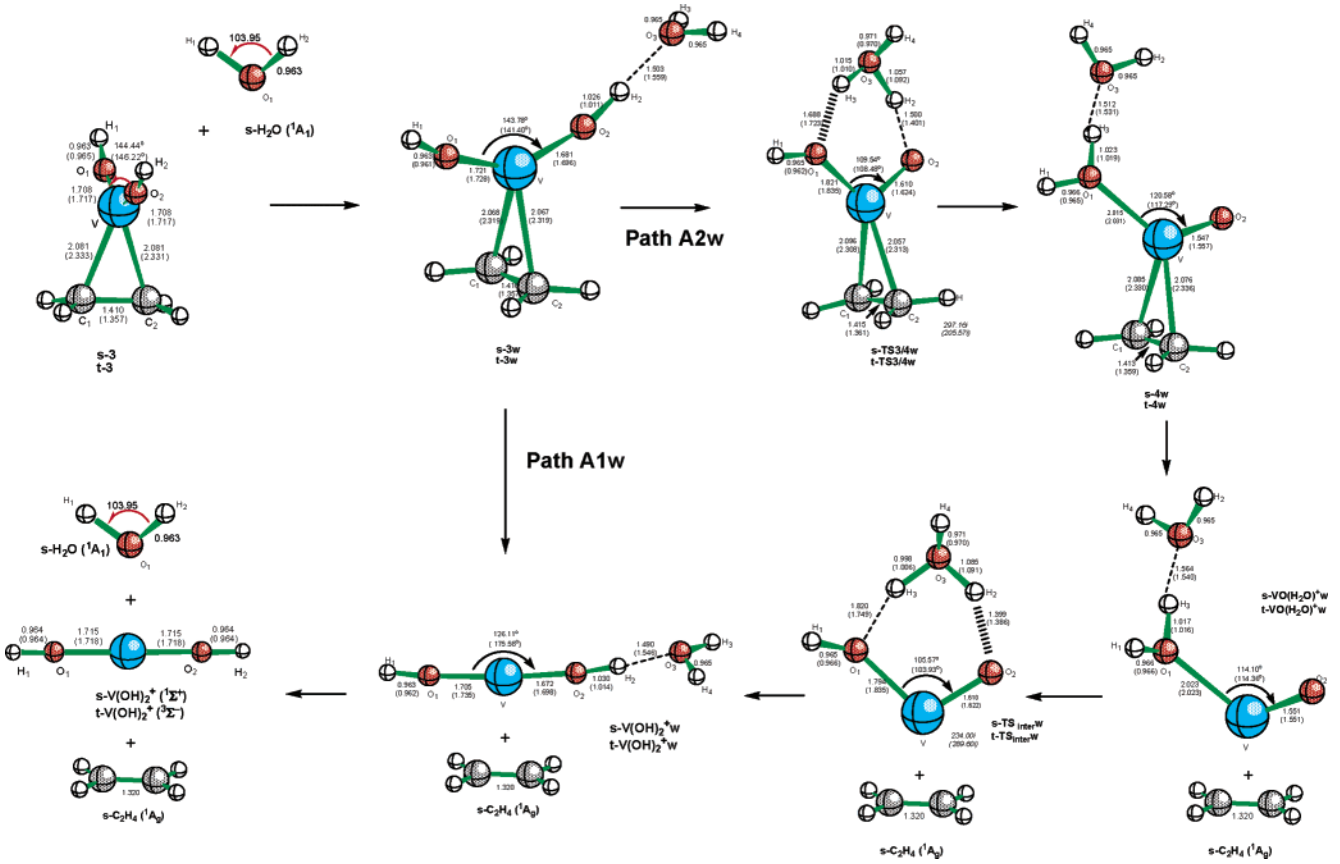

Figure 3. Structures (distances in Å and angles in deg) of the stationary points found in the singlet state and triplet state electronic (in parentheses) at the B3LYP/6311-G(2d,p) level along the paths A1w and A2w. For the TSs the imaginary vibrational frequencies (cm^{-1}) are shown in italics.

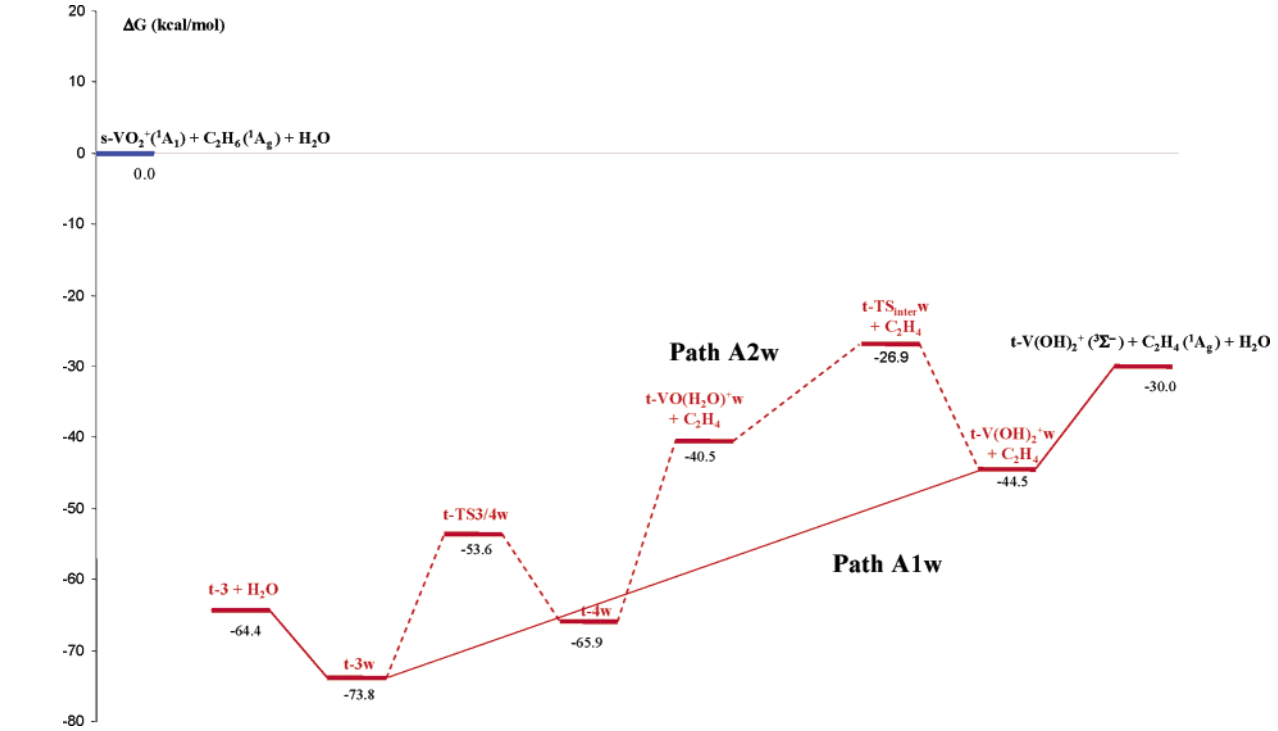

Figure 4. Gibbs free energy profiles at 298.15 K, relative to the reactants in the singlet electronic state, for the paths A1w and A2w.

while for both H atoms that are transferred in the isolated system the charge is 0.50 au. In this case, both **t-TS3/4w** and **t-TS$_{inter}$w** lie below the ground state asymptote.

We can propose two alternative channels, from the most stable reactants, **s-VO$_2^+$** + C_2H_6 + H_2O, to the most stable products, **t-VO$^+$** + $2H_2O$ + C_2H_4, including an additional water molecule: path A1w: **s-1**, **s-TS1/2**,

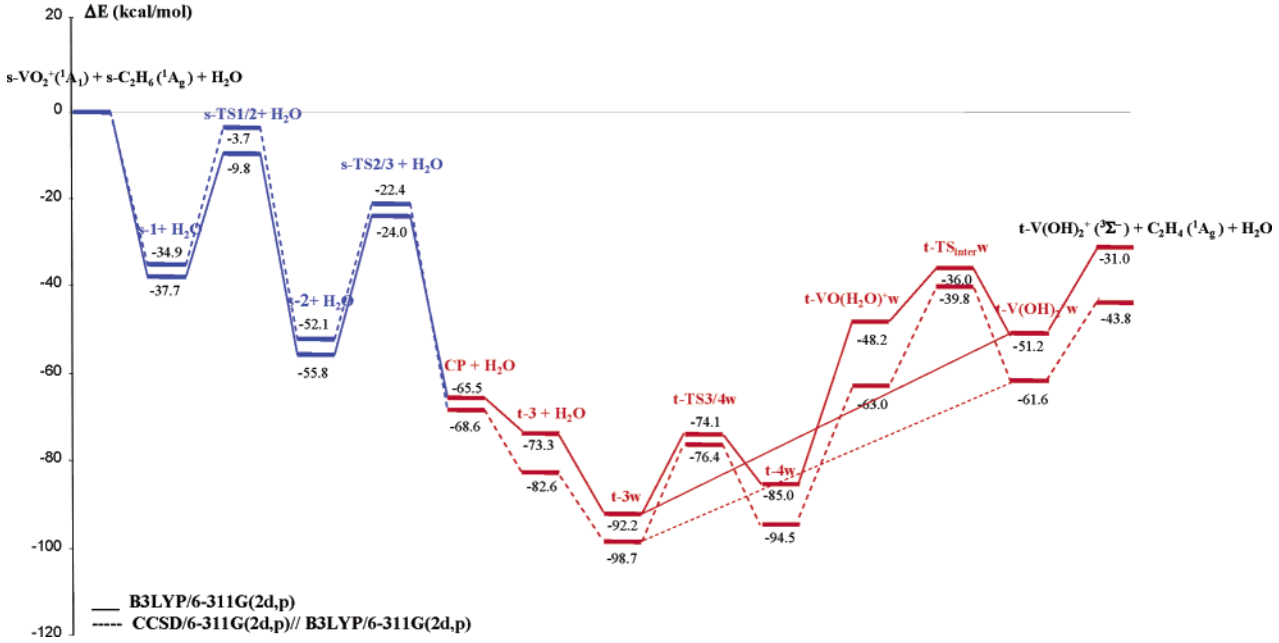

Figure 5. Relative energies, ΔE (kcal/mol), at the B3LYP/6-311G(2d,p) (solid line) and CCSD/6-311G(2d,p)//B3LYP/6-311G(2d,p) (dashed line) levels for the stationary point along paths A1w and A2w.

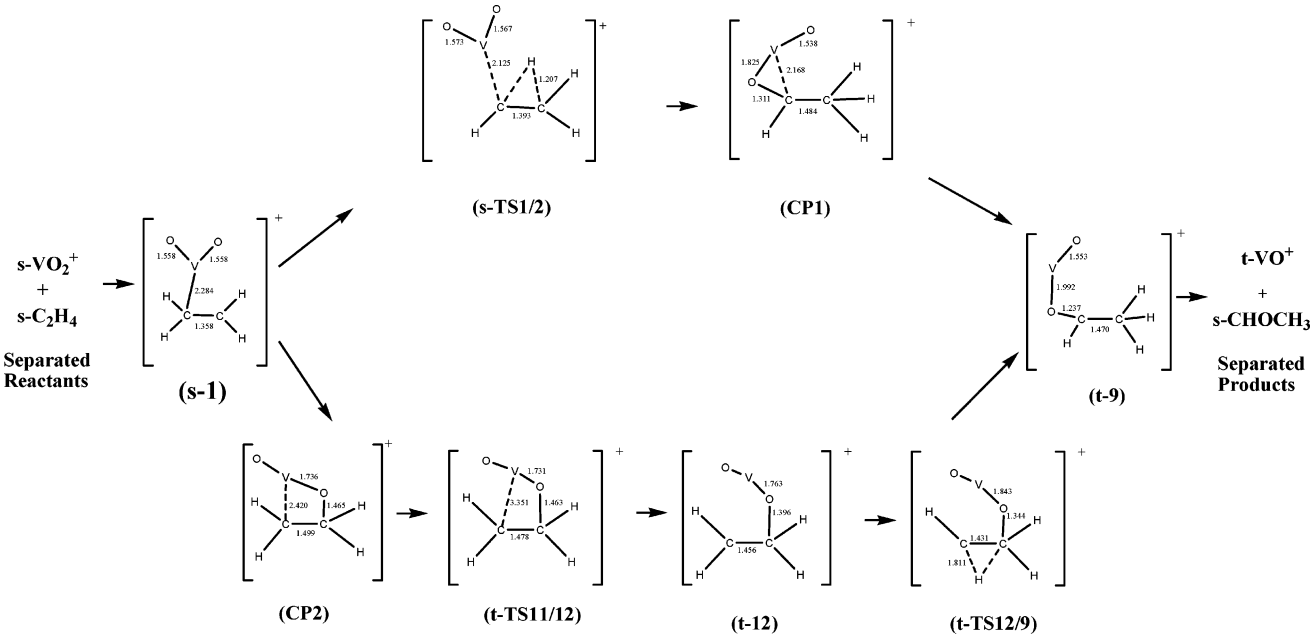

Figure 6. Structures of stationary points along the most favorable reaction pathways for the reaction **s-VO_2^+** + C_2H_4 to render **t-VO^+** + $CHOCH_3$.

s-2, **s-TS2/3**, **CP**, **t-3w** and path A2w: **s-1**, **s-TS1/2**, **s-2**, **s-TS2/3**, **CP**, **t-3w**, **t-TS3/4w**, **t-4w**, **t-VO(H_2O)$^+$w**, **t-TS_{inter}w**, **t-V($OH)_2^+$w**. In these paths all the stationary points lie below the ground state of the entrance channel, separated reactants. Therefore, these results point out that the reaction path A1w and path A2w, including the active participation of a discrete water molecule, can be considered as competitive.

Single-point CCSD/6-311G(2d,p)//B3LYP/6-311G(2d,p) calculations have been carried out on the most relevant stationary points along the A1w and A2w reaction channels. The energetic values obtained are schematically depicted in Figure 5. A comparison of Figures 2 (values of ΔG) and 5 (values of ΔE) shows that the decrease in ΔG is smaller than the decrease of ΔE due to the entropic term, which disfavors the formation of cyclic structures. An analysis of the results of Figure 5 shows the slight differences between the stationary points in the entrance channel, the intermediates, TSs, and **CP**. A larger difference is found for **t-VO(H_2O)$^+$w** (14.8 kcal/mol), **t-V($OH)_2^+$w** (10.4 kcal/mol), and the final products (12.8 kcal/mol).

3.3. Reaction $VO_2^+ + C_2H_6$ versus $VO_2^+ + C_2H_4$. In Figure 6, the most favorable reaction pathway for the rearrangement of $VO_2^+ + C_2H_4$,[96] which yields preferentially $CH_3CHO + VO^+$ ($^3\Sigma$), is depicted. An analysis and comparison between the previous reaction and the present study, $VO_2^+ + C_2H_6$ (which gives exclusively $V(OH)_2^+$ ($^3\Sigma^-$) + C_2H_4), show that a different reactivity pattern can be assigned to the initial interac-

tion complex of the reactants. In the case of the $VO_2^+ + C_2H_4$ reaction, a covalent interaction between V and one C atom of the ethane fragment is found (**s-1**); this stable complex determines the following behavior of the system. Therefore, the next steps are associated with an O atom transfer between V and C atoms and 1,2-hydride transfers between both carbon atoms. However, in the reaction of VO_2^+ with C_2H_6, the V atom forms a complex with the ethane fragment, avoiding the formation of a V−C bond along the reaction pathway. This result suggests that the origin of these reactivity patterns is in the intrinsic properties of alkane and alkene, avoiding in this first case the formation of a three-membered ring between the C−V−C frame. Therefore, two types of hydrogen transfer processes take place: (i) β-elimination from the ethane to vanadyl frameworks and (ii) tautomerization processes between the hydrated vanadium oxide, $VO(H_2O)^+$, and vanadium dihydroxide, $V(OH)_2^+$, fragments.

Finally, let us now consider the role of the switch from the triplet to singlet PESs. The crossing between them takes place in different regions along the most favorable reaction pathways. In the case of the reaction of VO_2^+ with C_2H_4 (see Figure 6), two CPs are characterized: (i) **CP1**, in the path from **s-TS1/2**, associated with the 1,2-hydride transfer, the cleavage of a C−V bond, and concomitant C−O bond formation to yield **t-9**; (ii) **CP2**, in the entrance channel in the path connecting the first intermediate, **s-1**, and **t-TS11/12**, associated with a C−V bond cleavage and C−O bond formation. In the reaction of VO_2^+ with C_2H_6 (see Figure 1), the **CP** occurs in the path connecting **s-TS2/3**, associated with the second C−H activation process, to the most stable minima, **t-3**.

3.4. Reaction of $VO_2^+ + C_2H_6$ versus $VO_2^+ +$ Propane. During the preparation of the final version of the present paper, Engeser et al.[97] performed computational investigations for the reaction between VO_2^+ and propane to yield propene elimination (path a1-1) and an ionic allyl complex (η^3-C_3H_5)V(O)-$(OH)^+$ along a dehydrogenation process (path a2). This work combines experimental and theoretical studies in order to elucidate some of the mechanistic intrigues of this reaction and provides an explanation for the elimination reaction between VO_2^+ and ethane to render ethene. Therefore, a comparison and an analysis between the present results and those reported by Engeser et al.[97] are mandatory, and in particular, the structures and energetic data of the stationary points along the reaction pathway A1 are reported in Figures 1 and 2 of this work. The path a1-1 to render propene and $V(OH)_2^+$ is similar to our results: the s and t electronic states cross between the second transition structures associated with the C−H activation process, **TS5/8**, and the global minima, **8**. Therefore, if spin inversion is easy, the propene elimination (path a1-1) is favoured with respect to dehydrogenation (path a2). These authors do not characterize the CP, and they point out that the switch between the spin states should control the outcome of the oxidation of propane by VO_2^+ along path a1. A comparison of the optimized geometry of the stationary points along paths a1-1 and A1 shows similar trends; while the values of the relative energies with respect to separated reactants reported by Engeser et al. show that the stationary points (minima, **4**, **5**, and **8**, and transition structures **TS4/5** and **TS5/8**) are more stabilized than our analogous systems (**s-1**, **s-2**, **t-3**, **s-TS1/2**, **s-TS2/3**, respectively), the values of the barrier heights between them are similar.

4. Conclusions

The present calculations using density functional theory, B3LYP/6-311G(2d,p), provide thermochemical and kinetic information on the reaction of VO_2^+ ($^1A_1$/$^3A''$) + C_2H_6 (^1A_g) to yield $V(OH)_2^+$ ($^1\Sigma^+/^3\Sigma^-$) + C_2H_4 (^1A_g) or VO^+ ($^1\Delta/^3\Sigma$) + H_2O ($^1A_1$) + C_2H_4 (^1A_g) and may thus provide a helpful tool for the interpretation of the experimental findings and an useful guide for understanding the mechanism of other analogous reactions. The results of the present study lead to the following conclusions: (i) the most kinetically and thermodynamically favorable reaction pathway takes place from **s-VO_2^+** + C_2H_6 reactants to **t-$V(OH_2)^+$** + C_2H_4 products. The first step corresponds to an insertion process of **s-VO_2^+** in the single C−C bond along a barrieless energy profile and an intermediate involving a cation (VO_2^+)−(C_2H_6) interaction complex, **s-1**. From this minimum, two consecutive C−H bond activation processes take place, associated with the hydrogen transfers (**s-TS1/2** and **s-TS2/3**) from the carbon to the oxygen atoms of the ethane and vanadyl cation frameworks, respectively. (ii) In the second C−H activation process, via **s-TS2/3**, to obtain the global minimum in the VO_2^+/ethane system, **t-3**, a crossing point, **CP**, has been characterized, and the following steps occur preferentially in the triplet electronic state. Therefore, the presence of **CP** should control the outcome of the reaction. **t-3** is an interaction complex between **t-$V(OH)_2^+$** and C_2H_4 frameworks and can be considered as a branching point because from this structure two alternative channels can be achieved: path A1 corresponds to a dissociation path to render the final products, and path A2 corresponds to two consecutive tautomerization processes between the dihydroxide cation, **t-$V(OH)_2^+$**, and the hydrated oxide cation, **t-$VO(H_2O)^+$**, associated with 1,3-hydrogen shifts. (iii) Path A2 is hindered by the large value of the corresponding barrier heights of these tautomerization processes, via **t-TS3/4** and **t-TS_{inter}**. (iv) An analysis of the Gibbs free energy profiles points out that along the most favorable reactive channel, A1, all stationary points lie below the ground state asymptote of the entrance channel, **s-VO_2^+** and C_2H_6, and the TS corresponding to the first C−H activation, **s-TS1/2**, presents the largest value of the relative Gibbs free energy. (v) Our calculations indicate that the participation of a discrete water molecule, along the A2w path, plays an important role, lowering the tautomerization barrier between dihydroxide cation, **t-$V(OH)_2^+$**, and hydrated oxide cation, **t-$VO(H_2O)^+$**, and making the isomerization easier. In this case paths A1w and A2w can be considered as competitive.

Acknowledgment. This work is supported by DGI (project BQU2000-1425-C03-02) as well as by Fundació Caixa Castelló-Bancaixa (projects P1A2002-04/05) and Brazilian Funding Agencies FAPESP, CAPES, and FUNDUNESP. L.G. is grateful to the Ministerio de Ciencia y Tecnología for doctoral fellowships. J.R.S. was

a visiting professor at Universitat Jaume I and acknowledges Fundació Caixa Castelló-Bancaixa, FAPESP, and CAPES for financial support. Computer facilities of the Servei d'Informàtica (Universitat Jaume I) and "Laboratório de Simulação Molecular", Unesp, Bauru, Brazil, are also acknowledged.

Supporting Information Available: Energies, geometries, and natural population analysis of all stationary points localized are summarized in S1−S47. This material is available free of charge via the Internet at http://pubs.acs.org.

OM0342098